

Review

Dry Reforming of Ethanol and Glycerol: Mini-Review

Jie Yu ^{1,*}, José A. Odriozola ^{2,3}  and Tomas R. Reina ² 

¹ State Key Laboratory of Coal Combustion, Huazhong University of Science and Technology, Wuhan 430074, China

² Department of Chemical and Process Engineering Department, University of Surrey, Guildford GU2 7XH, UK; odrio@us.es (J.A.O.); t.ramirezreina@surrey.ac.uk (T.R.R.)

³ Departamento de Química Inorgánica, Universidad de Sevilla, Instituto de Ciencias de Materiales de Sevilla Centro mixto US-CSIC Avda. Américo Vespucio 49, 41092 Seville, Spain

* Correspondence: yujie@hust.edu.cn

Received: 12 November 2019; Accepted: 28 November 2019; Published: 2 December 2019



Abstract: Dry reforming of ethanol and glycerol using CO₂ are promising technologies for H₂ production while mitigating CO₂ emission. Current studies mainly focused on steam reforming technology, while dry reforming has been typically less studied. Nevertheless, the urgent problem of CO₂ emissions directly linked to global warming has sparked a renewed interest on the catalysis community to pursue dry reforming routes. Indeed, dry reforming represents a straightforward route to utilize CO₂ while producing added value products such as syngas or hydrogen. In the absence of catalysts, the direct decomposition for H₂ production is less efficient. In this mini-review, ethanol and glycerol dry reforming processes have been discussed including their mechanistic aspects and strategies for catalysts successful design. The effect of support and promoters is addressed for better elucidating the catalytic mechanism of dry reforming of ethanol and glycerol. Activity and stability of state-of-the-art catalysts are comprehensively discussed in this review along with challenges and future opportunities to further develop the dry reforming routes as viable CO₂ utilization alternatives.

Keywords: CO₂ utilization; dry reforming; ethanol; glycerol; catalyst

1. Introduction

Carbon dioxide is one of the key greenhouse gases causing the observed global warming. Therefore, more attention has been given to the utilization of renewable energy and CO₂ recycling technologies. It is mainly from the combustion of fossil fuels since the Industrial Revolution age. In 1750, the CO₂ concentration in the atmosphere was 277 ppm according to Joos et al. and reached concentrations as high as 406.7 ppm in July 2017 [1]. However, CO₂ emissions have been found to be constant for the last three years as shown Figure 1a according to the International Energy Agency, proving the effect of the global effort regarding environmental policies.

Carbon capture and storage is regarded as a main method to limit CO₂ release in the atmosphere; nevertheless, this technology has not demonstrated commercial viability so far. A more challenging alternative from the chemical and engineering perspective is the carbon capture and recycling (CCR) approach, where CO₂ is converted and recycled back to fuels and added value chemicals.

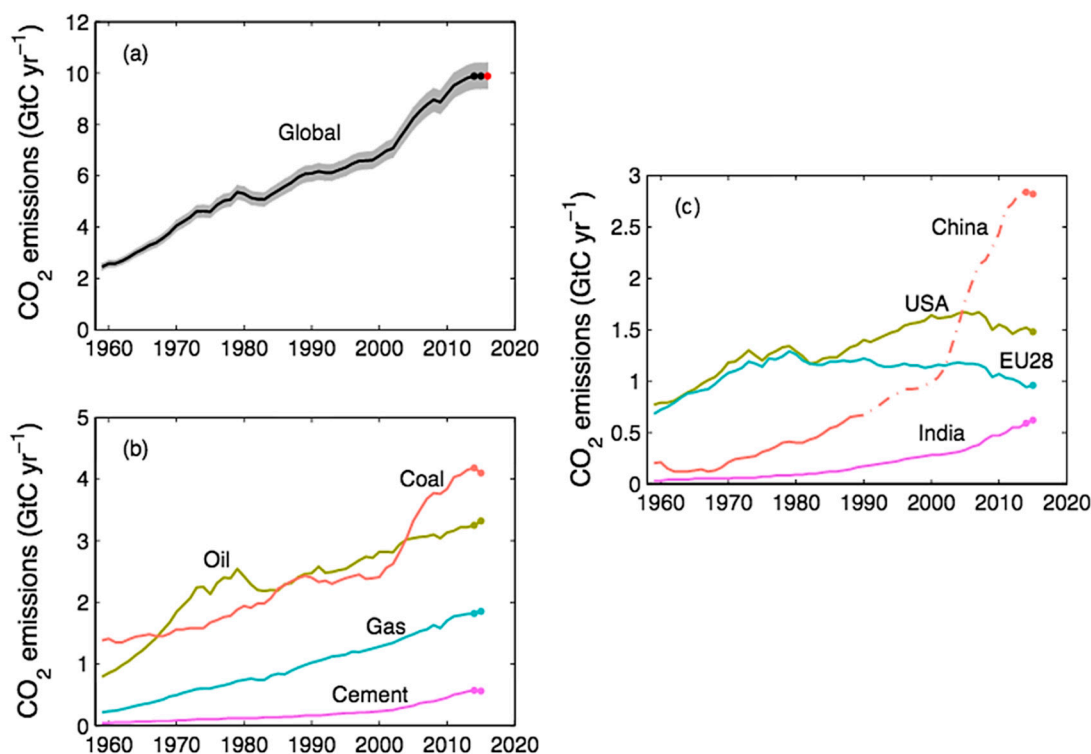


Figure 1. CO₂ emissions from fossil fuels and industry for (a) the globe (grey shading); (b) global emissions by fuel type; (c) territorial CO₂ emissions for USA, China, India, and for the EU—reproduced from Le Quéré et al. [2].

CO₂ can react with methane following the reaction of dry reforming of methane reaction (DRM) forming syngas. Syngas contained a mixture of carbon monoxide and hydrogen, which is a crucial raw compound in the chemical industry. Applications of synthesis gas are summarized in Figure 2. It can be used as base material for methanol synthesis (Equation (1)) that can later be upgraded to higher commercial value chemicals such as dimethyl ether (DME), formaldehyde or acetic acid. When introduced into a Fisher–Tropsch unit, syngas can produce fuels or waxes (Equation (2)). Finally, it can be rearranged into methane (Equation (3)) or used as a hydrogen source:

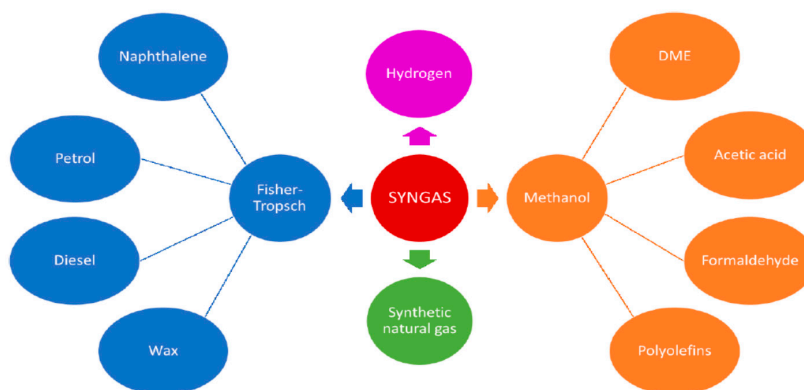
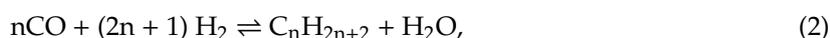


Figure 2. Applications of syngas.

Bio-ethanol, as a renewable biofuel, has been proposed as a substitute for fossil fuels. First generation of bio-ethanol was produced from food and was also heavily criticized since it opened the dilemma “food or fuel”. Currently, the second generation of bio-ethanol is mainly from lignocellulosic biomass residues and organic municipal solid waste with more complicated methods in order to avoid the consumption of food as shown in Figure 3. Therefore, bio-ethanol can be regarded as nearly CO₂ neutral. In 2018, the total production of bio-ethanol reached 28,700 million gallons and 83.7% is from USA and Brazil [3].

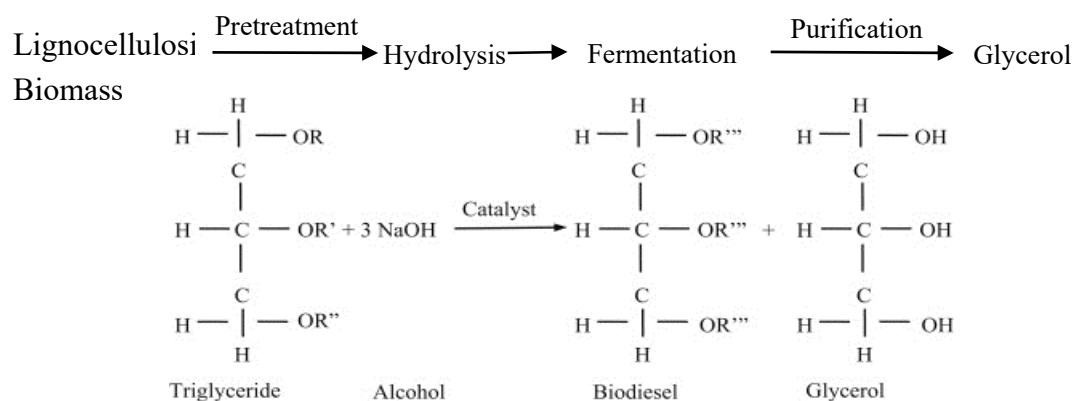


Figure 3. The pathway of production of bio-ethanol and glycerol.

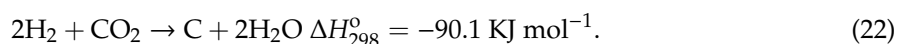
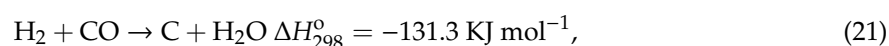
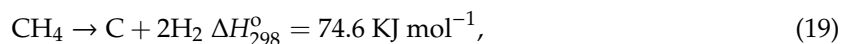
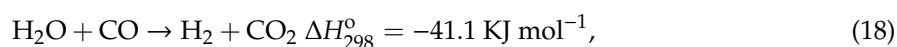
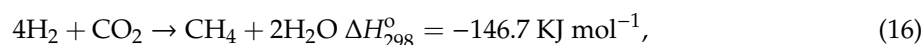
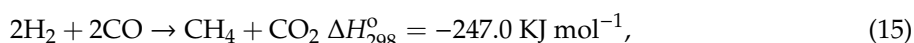
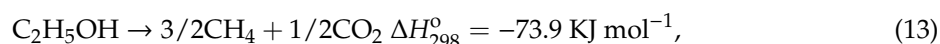
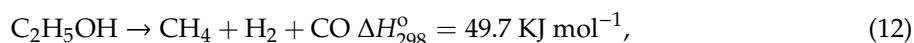
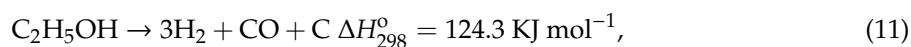
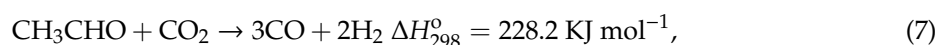
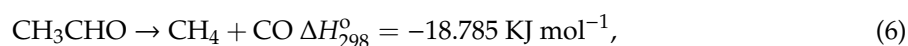
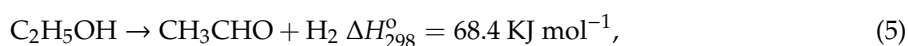
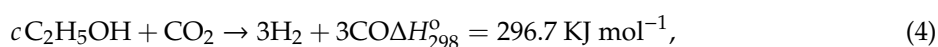
Biodiesel, the second most used biofuels after bio-ethanol, also attracted a wide amount of attention, which is mainly from the transesterification reaction of triglycerides. During the process, 1 kg of glycerol, the main by-product, was produced for 9 kg of biodiesel [4]. It was estimated that the production of glycerol each year can reach 4.2 million tons up to 2020 globally, while less than 3.5 million tons is needed each year [5]. Therefore, it is necessary to explore new market opportunities for glycerol.

A number of processes, such as pyrolysis and gasification with and without catalysts, have been developed to utilize bio-ethanol and glycerol [6–9]. To effectively close the carbon cycle, dry reforming of bio-ethanol and glycerol to produce syngas or H₂, which can be used directly or converted into high value chemical compounds were proposed [10–13]. Dry reforming normally occurs at relatively high temperatures (900–1200 K) in the existence of CO₂. The process involved several parallel reactions, including direct cracking, water gas shift reaction (WGSR), and methanation reactions, which may affect the final products. Therefore, extensive studies have been conducted to understand the dry reforming pathways of bio-ethanol and glycerol and try to maximize the production of H₂ [14,15]. Various catalysts, such as Ni, Rh, and Cu-based, were also proposed to optimize the reaction pathways to avoid the formation of undesired by-products and hinder the formation of carbon on the catalyst.

2. Dry Reforming of Ethanol

The simulation of dry reforming of ethanol by thermodynamic analysis has been studied to determine optimum conditions for H₂ production [16–18]. Figure 4 showed the variation of gas composition with temperature. For the studied temperature ranges, H₂ and CO increase linearly with temperature from 823 to 1123 K reflecting the endothermic character of the reforming reaction. According to Equation (4), an equal amount of H₂ and CO can be formed from the ethanol dry reforming. However, the thermodynamic analysis predicted that ethanol can be completely converted to H₂, CO, CH₄, CO₂, H₂O, and C. In addition, CH₃CHO may be formed by a dehydrogenation reaction following Equation (5). The formed CH₃CHO can be further decomposed into CH₄ and CO (Equation (6)) or reformed into H₂ and CO (Equation (7)). The CH₃CHO can also be dehydrated into C₂H₄ (Equation (8)) or ether Equation (9). Carbon deposition was predicted to happen especially in the low temperature window with a slight decrease of solid carbon formation when temperature is increased. Above 1100

K, ethanol was completely transformed into H₂, CO, and C. According to Equation (10), ethylene polymerization can partially form the carbon. The ethanol can also decompose into CO, H₂, CH₄, and acetone directly (Equations (11)–(14)). The formed CO and H₂ can be transformed into methane according to Equations (15) and (16). The DRM is strongly endothermic and can produce hydrogen and carbon monoxide (Equation (17)). At lower temperatures, WGSR, an exothermic and reversible reaction, can favor the production of hydrogen and carbon oxide (Equation (18)). The carbon residues can also be formed following decomposition of methane, Boudouard reaction, and reduction of CO (Equations (19)–(22)). According to the thermodynamics, a two-step reaction mechanism was then proposed for the dry reforming of ethanol. Initially, ethanol was directly decomposed into methane and acetaldehyde intermediates, which can be subsequently reformed to syngas [19,20]. Moreover, H₂O was predicted due to the reversed WGSR. Therefore, it is evident that ethanol reforming by CO₂ forming dominated for the whole temperatures ranges and other side reactions may also occur such as direct decomposition into methane, H₂/CO/C mixtures and C₂H₄O, methane reforming, and reverse WGSR:



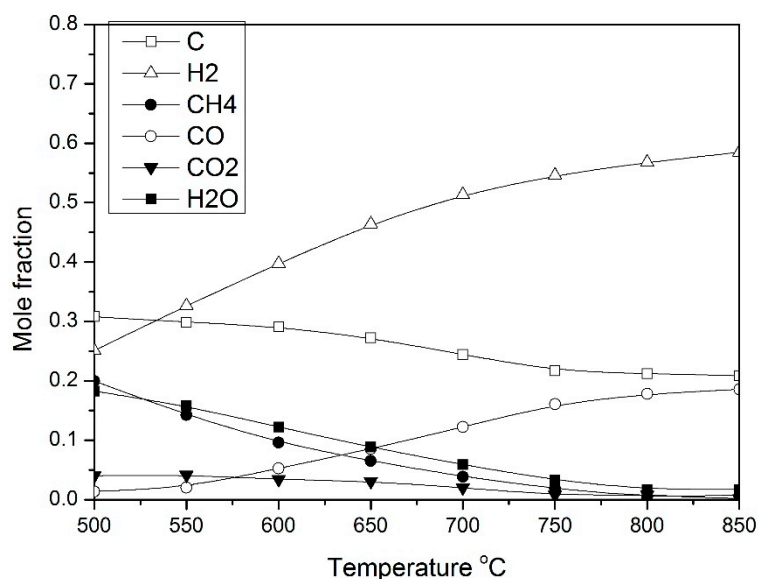


Figure 4. Equilibrium content of gas composition for the ethanol dry reforming process (Reproduced from [16]).

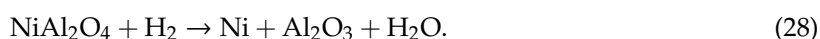
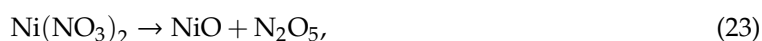
Thermodynamic analysis showed that the optimal conditions for dry reforming of ethanol are: reaction temperatures between 1200–1300 K, CO₂/ethanol ratios of 1.2–1.3. At these conditions, ~45% H₂, ~50% CO, and complete conversion of ethanol can be realized without remarkable solid carbon formation [21]. Ethanol conversion increased with the CO₂/ethanol ratio increasing, but kept almost constant at higher CO₂/ethanol ratios. A recent experimental study showed that ethanol conversion stabilized from CO₂/ethanol ratio of 1.4 [22]. Moreover, the H₂ in syngas also decreased at CO₂/ethanol higher than 1.4, while CO increased. This trend showcases the direct impact of the reversed WGS during the dry reforming processes as reported elsewhere [23–25].

In order to avoid the carbon formation and undesired gas components, different catalysts were synthesized and utilized for the dry reforming of ethanol, such as Ni, Cu, Rh, and Co based catalysts. The Ni based catalyst is the most studied one. Al supported nano-NiO-SiO₂ catalysts with Ni amount of 5, 7, 10, and 15% have been synthesized and used for the dry reforming of ethanol [26]. Catalysts containing 10% Ni showed the best activity partially due to the clustering of Ni particles at higher Ni amounts. Less CO and higher CH₄ were also observed due to higher rate of WGS and direct decomposition of ethanol into CH₄ promoted by the catalyst, respectively. The desired condition for dry reforming of ethanol was found at 1023 K with the ratio of CO₂/Ethanol being 1.4. At this condition, the conversion of CO₂ was observed to be 75%, while 100% conversion of ethanol was nearly obtained. Wei et al. used the Ni/KIT-6 (mesoporous silica) and Ni/SiO₂ for the dry reforming of ethanol [27]. A comparatively better activity and stability was shown for Ni/KIT-6 catalyst; however, Ni/SiO₂ was deactivated quickly. Complete ethanol conversion was obtained at 823 K for Ni/KIT-6 without observing clear deactivation of the catalyst after 40 h tests. Smaller particle size of Ni was observed for Ni/KIT-6, which can be stabilized by the confinement effect of catalyst channels.

The smaller particle size of Ni markedly hindered the carbon formation. The stronger interaction of metal-support also inhibited the sintering of active metals. Therefore, the catalyst of Ni/KIT-6 greatly inhibited the coke deposition and contributed to the superior activity. Catalysts of Ni/Y₂O₃-ZrO₂ using two different preparation methods of polymerization and wet impregnation were proposed for the dry reforming of ethanol at 600, 700 and 800 °C [10]. At 600 °C, the highest CH₄ was obtained using a 5%Ni/Y₂O₃-ZrO₂ catalyst, due to the direct cracking of ethanol into CH₄ and slow dry reforming rate of CH₄ at 600 °C. Increasing temperature to 700 °C accelerated the dry reforming rate of CH₄, which was then enhanced further at 800 °C. It was showed that stronger interaction between NiO and oxygen vacancies of support was responsible for its superior reforming ability. The preparation of

Ni/Y₂O₃-ZrO₂ catalyst by polymerization in one step was proven as an easier and superior way of loading Ni onto Y₂O₃-ZrO₂ support than by wet impregnation. In order to prevent the deactivation of Ni catalysts, Ni has also been incorporated into different supports of Al₂O₃, CeO₂, MgO and ZrO₂ to study their activity in the dry reforming of ethanol [28]. Ni-CeO₂ catalyst showed the best performance at 1023 K than at 973 K, suggesting that CO₂ conversion can be enhanced at higher temperatures, while carbon deposition was hindered. It was found that the reducibility of Ni, which was influenced by the interaction between support and Ni, along with the redox property of CeO₂ can promote the selectivity for H₂ and inhibit the unfavored side reactions. The results revealed that specific surface area of supports can affect the particle size and reducibility of active metals. It can be observed that interaction between Ni and the supports affected the particle size strongly, reducibility of Ni. Oxygen vacancy of support also can inhibit the formation of carbon.

To optimize the performance of Ni based catalysts, promoters such as La and Ce were also incorporated [11,19,29]. The advanced redox properties of Ce resulted in great benefits for a Ce-Ni/Al₂O₃ tested in the dry reforming of ethanol. Compared with unpromoted ones, Ce-promoted catalyst can hinder the formation of solid coke due to its oxygen mobility ascribed to CeO₂ as a promoter. The proportion of amorphous carbon as opposed to graphitic carbon was also observed with Ce-Ni/Al₂O₃. Upon incorporation of Ce, the interaction between Ni and the supports was strengthened, which can promote the formation of smaller NiO clusters facilitating the reducibility of Ni. The incorporation of Ce lowered reduction temperatures by around 315 K. NiO and NiAl₂O₄ were observed on the surface of the supports during calcination while CeO₂ was observed on the promoted one. The derivative weight of calcination and H₂-temperature program reduction (H₂-TPR) of two catalysts was shown in Figure 5, respectively. As shown in Figure 5a, the first peak, P1 (at 501–509 K), was caused by the direct decomposition of metal nitrates forming the corresponding metal oxides (Equations (23) and (24)). The second peak (P2) (591–598 K) was ascribed to NiAl₂O₄ formation (Equation (25)). The third peaks (P3) of Ce-promoted catalyst (661 K) was due to the transformation of Ce³⁺ to Ce⁴⁺ during calcination (Equation (26)). In Figure 5b, two distinct peaks were observed for the H₂-TPR analysis of catalysts. The P1 (557–599 K) was due to the formation of metallic Ni from the reduction of NiO (Equation (27)), while P2 peak (668–671 K) was due to the transformation of NiAl₂O₄ to Ni (Equation (28)):



Similarly, La has also been incorporated into Ni/Al₂O₃ [11,20]. La can enhance the dispersion of nickel particle and hinder the agglomeration of active phases. The best performance of dry reforming of ethanol was observed at 3% La loading due to the benefits of La₂O₃ as promoter. The H₂-TPR analysis of three catalysts were shown in Figure 6. Different from Ce promoted Ni/Al₂O₃, three peaks were observed for 3%La-10%Ni/Al₂O₃. The first one, P1, was due to the reduction of NiO to metallic Ni form. The second peak P2 was due to the reduction of NiO particles strongly absorbed by supports. The third peak P3 was due to the reduction of spinel NiLa₂O₄ phase to elementary Ni. For 10%Ni/Al₂O₃ and 3%La-10%Ni/Al₂O₃, the temperature for NiO reduction (P1 and P2) decreased to a lower value after La loading, which may be ascribed to the transferring electrons from La₂O₃ to NiO particles. As a result, the enhanced electron density facilitated reduction of NiO. It was also found that dry reforming of ethanol may occur through direct decomposition of ethanol to methane intermediates. The formed intermediated were then reformed to a mixture of CO and H₂ following DRM. Similar to Ce promoted

catalyst, amorphous carbon dominated on the surface of used La-Ni/Al₂O₃ catalyst. This is may be due to the enhanced basicity of the promoted catalysts and the multiple oxidation states of La, which can provide a shortcut of coke conversion by redox reactions (Equations (29) and (30)).

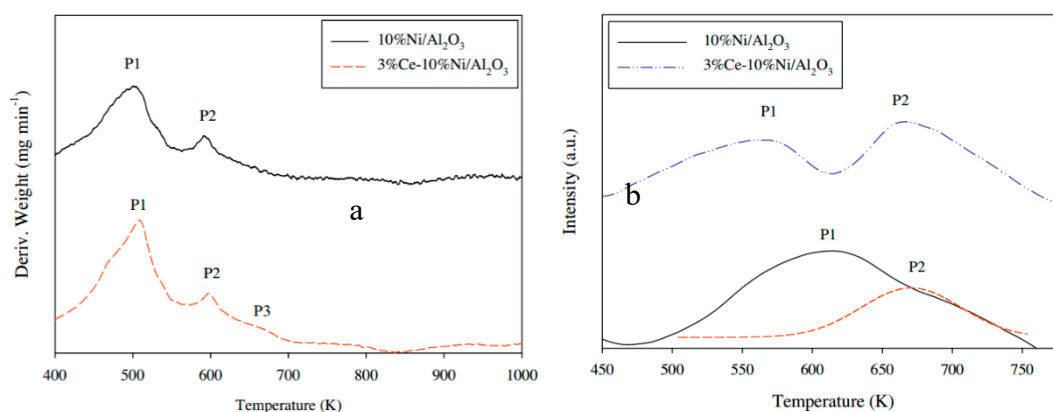
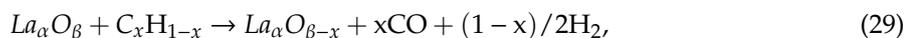


Figure 5. Derivative weight for temperature-programmed calcination (a) and H₂-TPR (b) 3%Ce-10%Ni/Al₂O₃ and 10%Ni/Al₂O₃ catalysts, reproduced with permission from [19].

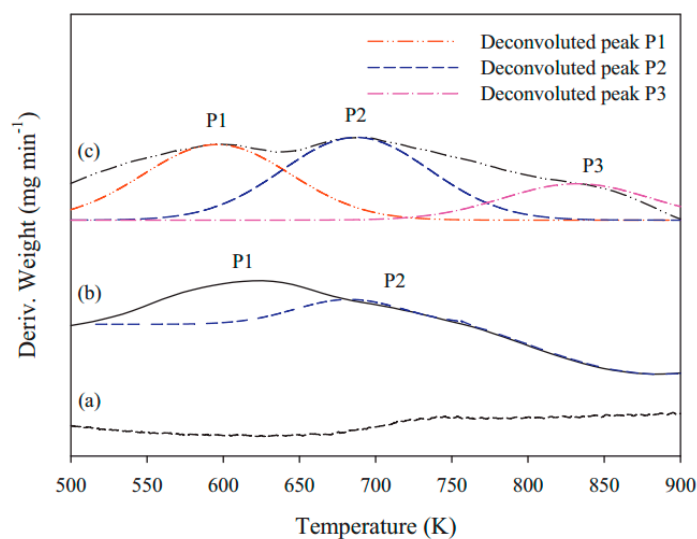


Figure 6. H₂-TPR (a) Al₂O₃, (b) 10%Ni/Al₂O₃ and (c) 3%La-10%Ni/Al₂O₃ catalysts, reproduced with permission from [11].

Co based catalysts promoted by Ce and La have also been proposed for the dry reforming of ethanol [30–32]. The addition of Ce and La facilitated the reduction of Co₃O₄ to CoO, which can be further transformed into Co. The reducibility of active metals in catalysts were analyzed using H₂-TPR. The reduction ability followed the order of 10%Co/Al₂O₃ < 3%Ce-10%Co/Al₂O₃ < 3%La-10%Co/Al₂O₃. Three peaks were observed. The first peak for all catalysts was due to the reduction of Co₃O₄ to CoO, while the second peak was ascribed to the formation of Co from CoO reduction. The third small shoulder was most likely ascribed to the reduction of pinel CoAl₂O₄ species strongly absorbed by support. Consistent with reducibility of catalysts, the dry reforming activity of ethanol followed the order of 3%La-10%Co/Al₂O₃ > 10%Co/Al₂O₃ > 3%Ce-10%Co/Al₂O₃. The relationship indicated

that the La and Ce can promote the amount of Co active sites by accelerating the reduction of Co_3O_4 demonstrating a clear correlation redox properties—catalytic performance.

The dry reforming of ethanol was proposed using Cu-based catalysts [33–36]. A catalyst of $\text{Cu/Ce}_{0.8}\text{Zr}_{0.2}\text{O}_2$ was prepared using the co-precipitation method. The synergistic interaction between metal and support along with the redox characteristic of Ce caused a promising activity. A new preparation method of the ball-milling technique was then proposed by the same group for dry reforming of ethanol. The catalyst synthesized by the ball-milling technique showed a better performance than the co-precipitation method, which can be ascribed to the better dispersion of Cu and optimized interaction between metal and support. Moreover, no encapsulated graphite-type carbon was found for this catalyst. In a further study, Cu-based catalysts on various supports (CeO_2 , ZrO_2 , $\text{CeO}_2\text{-ZrO}_2$) were synthesized. As revealed, the reducibility of Cu and oxygen vacancies decreased in the order of $\text{CuCeZr} > \text{CuCe} > \text{Cu/Zr}$. As expected, the CuCeZr catalyst showed the best performance due to higher metal dispersion, stronger interaction between metal and support, and greater concentration oxygen vacancies that are envisaged as reactive sites for molecules' activation. To prove the assumption, all catalysts were exposed to H_2 -TPR analysis as shown in Figure 7. For the supports, the incorporation of Zr^{4+} accelerated mobility of O and increased reducible Ce^{4+} cations. For Cu-based catalysts, the reduction started at about 100°C with the highest peaks at 142°C , 154°C and 162°C for CuCe, CuCeZr and CuZr, respectively. This is due to the stronger interaction between Cu and CeZr supports that can accelerate oxygen mobility. As a result, catalyst reduction temperature can be reduced.

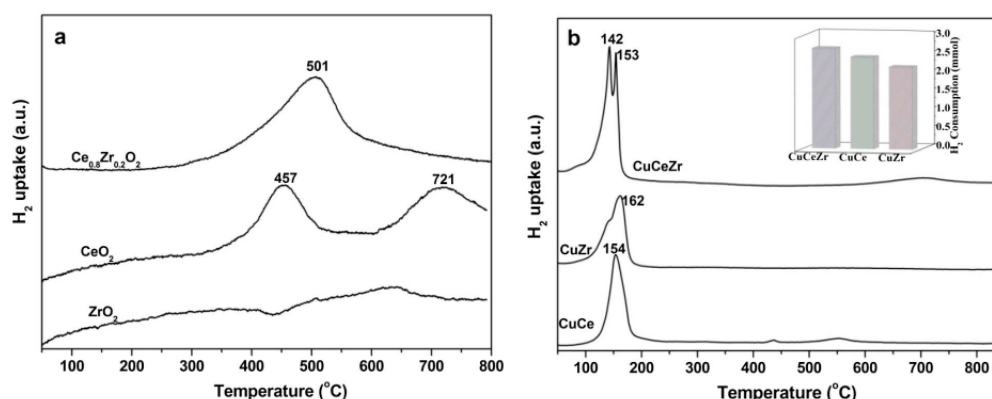


Figure 7. H_2 -TPR profiles of the as-prepared catalysts (a) supports; (b) Cu-based catalysts, reproduced with permission from [33].

Due to the high activity for C–C bond cleavage and low coke formation, Rh has been extensively used for dry reforming of methane [37]. To validate its applicability on the dry reforming of ethanol by Rh based catalysts, various Rh based catalysts have been prepared. Figure 8 shows that ethanol decomposition may occur by two major routes [38]: (1) forming an oxametallacycle intermediate on Rh(1,1,1), which was directly decomposed to methane and CO; and (2) dehydrogenated intermediates ($\text{C}_2\text{H}_4\text{O}$ and acetyl species), which can be further decomposed to CO and CH_x species.

Due to the proven redox property of CeO_2 , Rh/ CeO_2 has been synthesized for the dry reforming of ethanol [14,39]. A relatively good activity and stability were observed for this catalyst due to the interaction between Rh and CeO_2 and again the advanced redox features of CeO_2 , which can accelerate CO_2 activation and prevent carbon deposition. The mechanism was illustrated in Figure 9.

In further research, Rh/Ce-SBA-15 has been synthesized for the dry reforming of ethanol [40]. The proportion of Ce relative to Si affected markedly the H_2 production and selectivity. The introduction of Ce into the 1%Rh/SBA-15 increased reforming activity due to the strengthened mobility of oxygen species on the surface of catalysts. Rh-based catalysts were also prepared for the dry reforming of ethanol using $\text{MxO}_y\text{-Al}_2\text{O}_3$ oxides ($\text{M} = \text{Zr}, \text{Mg}, \text{Ni}, \text{Ce}, \text{La}$) as supports [41]. As shown in Figure 10, the production of H_2 followed the order: $\text{Rh/NiO-Al}_2\text{O}_3 \gg \text{Rh/Al}_2\text{O}_3 \approx \text{Rh/MgO-Al}_2\text{O}_3 \approx \text{Rh/CeO}_2\text{-Al}_2\text{O}_3$

> Rh/ZrO₂-Al₂O₃ ≈ Rh/La₂O₃-Al₂O₃. The superior performance of Rh/NiO-Al₂O₃ may be due to the existence of NiAl₂O₄ spinel phase, hindering the rhodium deactivation, and the high dispersion of Rh favored by co-existence of nickel particles.

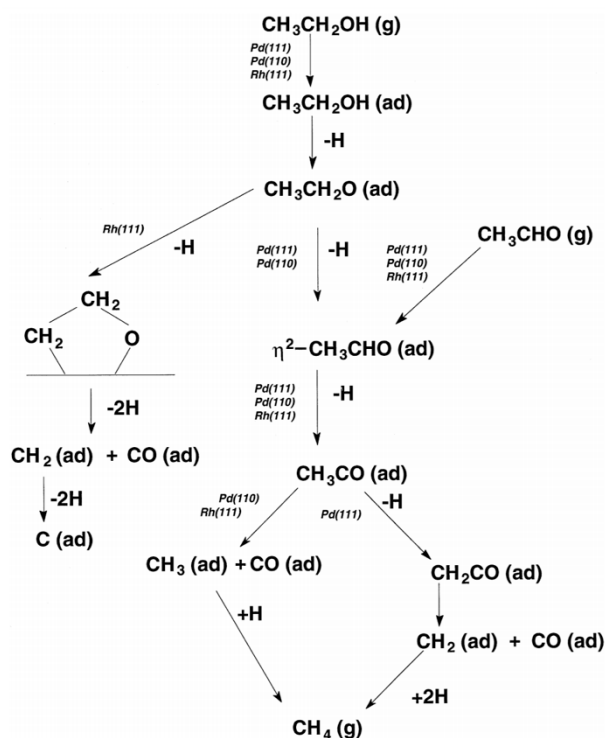


Figure 8. Reaction pathways observed for ethanol decomposition on Rh surfaces, reproduced with permission from [38].

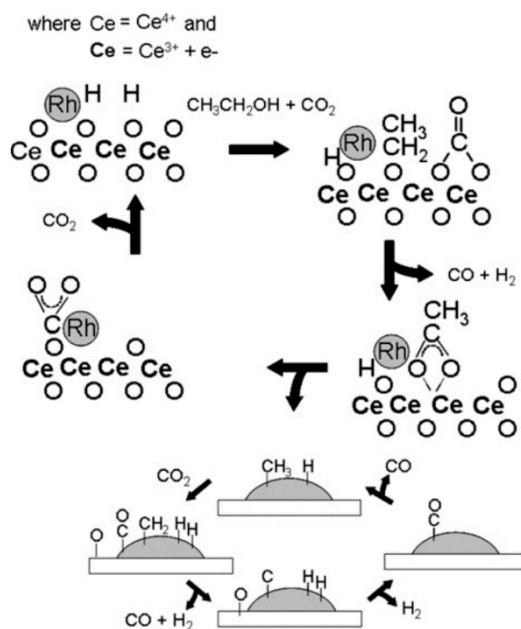


Figure 9. Reaction pathways observed for ethanol on Rh/CeO₂ surface, reproduced with permission from [14].

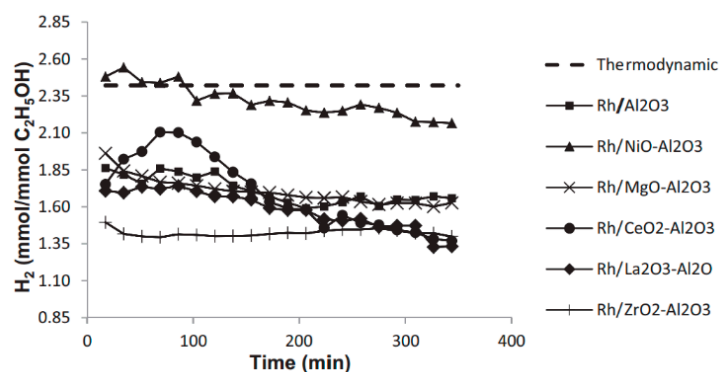


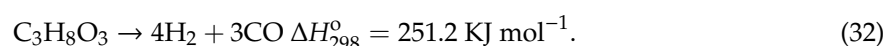
Figure 10. Evolution of H₂ yield of ethanol dry reforming reaction at 1073 K over different M_xO_y-Al₂O₃ supported Rh catalysts, reproduced with permission from [41].

The 316 steel (Fe: 61%; Cr: 16–18.5%; Ni: 10–14%; Mo: 2–3%; C: 0.03%) and carbon steel also proved the dry reforming activity of ethanol [42–44]. Compared with the conditions without catalyst, steel can promote the catalytic cracking and catalytic reforming of ethanol forming H₂ and CO. In this process, carbon nanofilament was formed as the desired product. It was proposed that nanoparticles of magnetite can be formed from the oxidation treatment prior to dry reforming reaction, which can be reduced into Fe₃C during the reforming process. The formed Fe₃C is responsible for the formation of H₂, CO, and nanofilament. Hence, a take-home message is to check the potential catalytic activity of the reactor itself and always run a blank test to rule out contributions beyond our catalytic materials.

In this part, various catalysts used for dry reforming of ethanol have been summarized. The most used catalyst is Ni based one due to its low cost even though other catalysts of Co, Cu, and Rh based have also been proposed. The most common problem is the deactivation of catalyst caused by coke formation. In order to minimize this effect, promoters of Ce and La were introduced, which showed a promising effect due to the redox properties of Ce and enhanced dispersion of Ni by Ce and La. Different catalyst supports were also discussed. The effect of support on performance is attributed to the interaction between support and active metals. Strong interaction between NiO and oxygen vacancies of catalyst can enhance the catalyst performance. In the ideal conditions, complete conversion of ethanol can be achieved with a theoretical amount of H₂ obtained. Therefore, dry reforming of ethanol is a promising technology to produce syngas.

3. Dry Reforming of Glycerol

The dry reforming of glycerol is expected to follow a similar pattern to that of ethanol. Theoretically, 3 mol of H₂ and 4 mol of CO can be extracted from 1 mol of dry reforming of glycerol according to Equation (31). However, direct decomposition of glycerol may also occur following the overall reaction as shown in Equation (32) along with methanation and (reverse) WGSRs. Thermodynamic analysis has been used to study the effect temperature, pressure, and CO₂/glycerol ratios on glycerol conversion [45,46]. It showed that atmospheric pressure is preferred for the glycerol conversion [47]:



As shown in Figure 11, temperature showed a positive effect on H₂ production, which reached a maximum conversion at CO₂/glycerol ratios higher than 1 due to the promoted reverse WGSR at higher CO₂ pressure. At a CO₂/glycerol ratio between 0 and 1 over 975 K, more than three moles of H₂ can be obtained, while more syngas (H₂ and CO) can be produced at higher temperatures and CO₂/glycerol ratios. The optimum condition for syngas production occurred at 1000 K with CO₂/glycerol ratio of 1, at which 6.4 mol of syngas (H₂/CO = 1:1) can be obtained for each mole of glycerol.

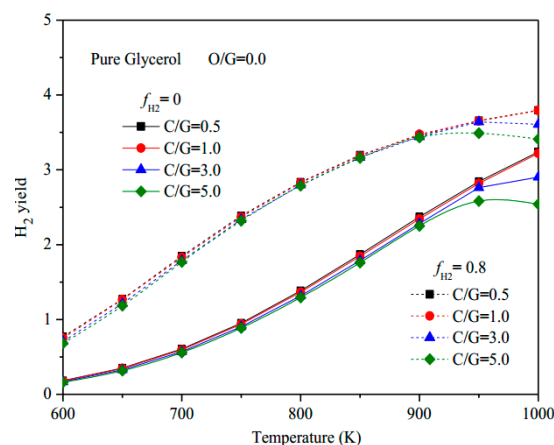


Figure 11. The effect of CGR ($\text{CO}_2/\text{glycerol}$ ratio) and temperature on H_2 production during the glycerol dry reforming process. f_{H_2} is hydrogen separation fraction, reproduced with permission from [46].

In the absence of catalysts, the glycerol conversion is low. To optimize H_2 production and reaction conditions, various catalysts have been synthesized for the dry reforming of glycerol. Mesoporous catalysts of $\text{Ni}/\gamma\text{-Al}_2\text{O}_3$ with different amounts of Ni were prepared for the dry reforming of glycerol [12]. With Ni amount increasing from 5 to 15%, the glycerol conversion increased, while it decreased at higher Ni content. The H_2 -TPR analysis showed that the higher Ni amount promoted the reducibility of the Ni catalyst, which can be related to lower dispersion of Ni at higher content of Ni. Other catalysts, including Rh, Ni, and Co based catalysts ($\text{Al}_2\text{O}_3\text{-ZrO}_2\text{-TiO}_2$ support) have been synthesized for the dry reforming of glycerol [4], with the particle size of Rh, Ni and Co being 3–4, 10–15, 40–50 nm, respectively. The highest activity was observed for Rh, while the activity of Co was the lowest. Even though the activity of Ni based catalyst was below that of Rh based catalyst, it can still render 95% of the thermodynamic CO_2 conversion at maximum. The high performance of Ni based catalyst may be due to its ability of gasifying deposited carbon and metallic nature during the reaction. Comparatively, Co based catalyst showed an inferior performance to Rh and Ni due to the sintering, carbon deposition and Co oxidation. To understand the mechanism, all catalysts were exposed to H_2 -TPR analysis as shown in Figure 12. $\text{Al}_2\text{O}_3\text{-ZrO}_2\text{-TiO}_2$ support showed a broad H_2 consumption in the high temperature region (i.e., 893–953 K), which is likely due to reduction of the $\text{Al}_2\text{O}_3\text{-ZrO}_2\text{-TiO}_2$ support. In addition to this high temperature peak, $\text{Rh}/\text{Al}_2\text{O}_3\text{-ZrO}_2\text{-TiO}_2$ revealed two more low-temperature H_2 consumption features at 160 and 200 °C, which can be attributed to the reduction of Rh^{3+} to Rh^+ and Rh^+ to metallic Rh species, respectively. $\text{Co}/\text{Al}_2\text{O}_3\text{-ZrO}_2\text{-TiO}_2$ also revealed two low temperature features with relatively lower H_2 consumption around 220–300 °C which can be ascribed to two-step reduction of Co_3O_4 to CoO and CoO to metallic Co. In addition, there exists a reduction feature at 420 °C, which can be ascribed to the reduction of CoO_x species that are strongly interacting with the $\text{Al}_2\text{O}_3\text{-ZrO}_2\text{-TiO}_2$ support material. $\text{Ni}/\text{Al}_2\text{O}_3\text{-ZrO}_2\text{-TiO}_2$ exhibited a similar H_2 consumption profile to that of $\text{Al}_2\text{O}_3\text{-ZrO}_2\text{-TiO}_2$ support and lacks a low temperature reduction peak (e.g., for $\text{Ni}^{+2} \rightarrow \text{Ni}^0$), indicating the presence of predominantly metallic Ni species on fresh samples with a negligible contribution from NiO and $\text{Ni}(\text{OH})_2$. For all catalysts, a negative effect of $\text{CO}_2/\text{glycerol}$ ratios between 1 and 4 on glycerol conversion was observed mainly due to the reverse WGS. For CO_2 conversion, the catalysts showed an increase in activity for $\text{CO}_2/\text{glycerol}$ ratio increasing from 1 to 2. However, CO_2 conversions decreased at higher ratios. This phenomenon has been observed by other researchers [13,48].

A similar study on dry reforming of glycerol by $\text{La-Ni}/\text{Al}_2\text{O}_3$ showed that glycerol conversion and H_2 generation rate reached a peak at $\text{CO}_2/\text{glycerol}$ ratio of 1.67, at which CH_4 reached the minimum. The existence of CH_4 in the presence of glycerol only, along with the declining trend at higher $\text{CO}_2/\text{glycerol}$ (>1.67), indicated that CH_4 may be formed from direct decomposition of glycerol, which can be then reformed by CO_2 to CO and H_2 . Regarding the H_2/CO ratio, the direct decomposition

of glycerol produced the highest value, but still below 2, which can be used in the Fischer–Tropsch process in some cases depending on the targeted end products. The declining trend with CO₂/glycerol ratio increasing may be caused by the reverse WGS. The noble metals (Rh, Ru, Ir, Pd, Pt) were also supported on MgAl₂O₄ and compared for dry reforming of glycerol [49]. Similarly, Rh showed highest activity and stability, which may be ascribed to high active metal areas. The catalytic activity followed the order: Rh > Ru > Ir > Pd > Pt. Cement clinker-supported Ni catalysts were also synthesized for the dry reforming of glycerol [50,51]. It was found that direct decomposition of glycerol was responsible for the H₂ production as opposed to a direct interaction between glycerol and CO₂ during reforming reaction. Therefore, even though the cement clinker can facilitate the adsorption of CO₂, it did not favor the production of H₂.

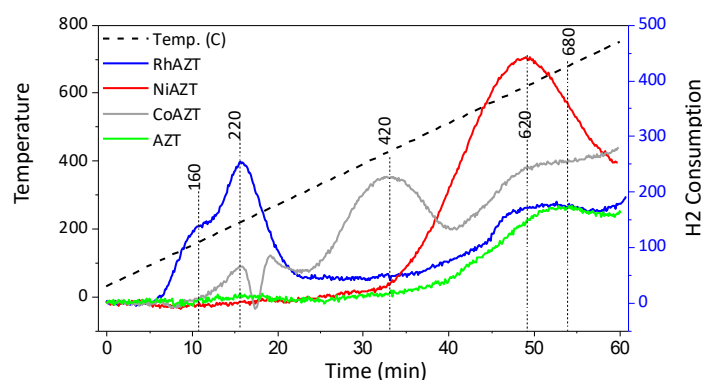


Figure 12. H₂-TPR data for fresh Al₂O₃-ZrO₂-TiO₂, Rh/Al₂O₃-ZrO₂-TiO₂, Ni/Al₂O₃-ZrO₂-TiO₂ and Co/Al₂O₃-ZrO₂-TiO₂ samples, reproduced with permission from [4].

To optimize the behavior of Ni based catalyst, La has been incorporated as a promoter for the dry reforming of glycerol [13,48,52,53]. After evaluating the effect of different content of La loaded, it was found that the glycerol conversion decreased in the order of 2%La-Ni/Al₂O₃ > 3%La-Ni/Al₂O₃ > 4%La-Ni/Al₂O₃ > 1%La-Al₂O₃ > Ni/Al₂O₃ > 5%La-Ni/Al₂O₃ > Al₂O₃. The main reason is that Ni metal can be better dispersed by La. However, when La content was above 2%, the clogging of pores may occur even though there is reduced particle size of Ni metals. Moreover, compared with the non-promoted catalyst, the La promoted catalysts showed a better carbon resistance due to its redox property to remove carbon and less acidity of Ni catalyst decreased by La. The promoters Re and Ag were also incorporated to optimize the performance of Ni based catalysts [54,55]. Similar to La, Ag can also improve the dispersion of Ni metals. However, at a high content of 5% Ag in catalyst, some active metal surface may be covered by Ag, which can decrease the catalyst performance. Differently, the Re can increase the glycerol conversion by enhancing the surface adsorption of OH group of the glycerol.

Rh based catalysts (Rh/ZrO₂ and Rh/CeO₂) were also synthesized for dry reforming of glycerol [15]. A declining trend of glycerol conversion and H₂/CO ratios with CO₂/glycerol increasing were also observed for the studied catalysts. Rh/ZrO₂ deactivated faster than Rh/CeO₂, due to the sintering of Rh metals and coke formation.

The dry reforming of glycerol with and without catalysts were summarized in this part. Without a catalyst, the production of H₂ from glycerol was low. For the various catalysts, including Ni, Rh, and Co, the highest activity was observed for Rh, while the activity of Co was the lowest. For the noble metals, the catalytic activity followed the order: Rh > Ru > Ir > Pd > Pt. Therefore, it can be concluded that Rh based catalysts showed a superior performance, especially on CeO₂ support. The La was also reported to promote the activity of active metals due to its redox property to remove carbon and less acidity of the Ni catalyst. Even though the conversion of glycerol is lower than ethanol generally, the glycerol conversion can still reach 90% in the presence of Rh/Al₂O₃-ZrO₂-TiO₂. The summarization showed the promising way of dry reforming of glycerol in the well-designed catalysts for H₂.

The dry reforming of ethanol and glycerol were summarized in Table 1.

Table 1. Summary of dry reforming of ethanol and glycerol using different catalysts.

| Active Metals | Supports | Promoters | Sample | Comments |
|---------------|--|-----------|----------|---|
| Ni | SiO ₂ | | Ethanol | Clustering of Ni may occur at high Ni loading [26]. |
| | SiO ₂ , KIT-6 | | | Stronger interaction of Ni-support inhibited the sintering of Ni [27]. |
| | Y ₂ O ₃ -ZrO ₂ | | | Stronger interaction between Ni and oxygen vacancies of support accelerated the activity. |
| | Al ₂ O ₃ , CeO ₂ , MgO and ZrO ₂ | | | Ni-CeO ₂ catalyst showed the best performance. Redox property of CeO ₂ can promote the selectivity for H ₂ and inhibit the unfavored side reactions [10]. |
| | Al ₂ O ₃ | Ce | | Ce-promoted catalyst can inhibit the formation of carbon due to its oxygen mobility of CeO ₂ [28]. |
| | Al ₂ O ₃ | La | | La can enhance the dispersion of Ni particle and hinder the sintering of metal oxides [29]. |
| Co | Al ₂ O ₃ | Ce, La | | La and Ce can increase the number of Co active sites by accelerating the reduction of Co ₃ O ₄ [30–32]. |
| Cu | CeO ₂ , ZrO ₂ | Ce | | CuCeZr catalyst showed the best activity and stability due to higher Cu dispersion, strong metal support interaction and more oxygen vacancies [33–36]. |
| Rh | SBA-15 | Ce | | The interaction between Rh and CeO ₂ and strong redox capacity of CeO ₂ can accelerate of CO ₂ activation and prevent carbon deposition [40]. |
| | Al ₂ O ₃ , MgO-Al ₂ O ₃ , ZrO ₂ -Al ₂ O ₃ | Ce, La | | The superior performance of Rh/NiO-Al ₂ O ₃ is due to the presence of NiAl ₂ O ₄ spinel phase, and high dispersion of Rh [41]. |
| Ir | Ce _{0.75} Zr _{0.25} O ₂ | | | The dispersion, reducibility of Ir, oxygen vacancies of supports and interaction between Ir and support decreased with the calcination temperature increasing. IrCeZr550 catalyst (calcination at 823 K) exhibited a satisfactory performance with high activity and stability. Increasing calcination temperature up to 850 °C decreased markedly the interaction between Ir and support, dispersion and reducibility of Ir, and the dissociation capacity of the C-C bond [56]. |
| Ni | Al ₂ O ₃ | | Glycerol | The glycerol conversion increased for Ni from 5 to 15%, while decreased at higher Ni, which may be related to lower Ni dispersion at higher content of Ni [12]. |
| | Al ₂ O ₃ | La | | Glycerol conversion and H ₂ generation rate reached a peak at CO ₂ /glycerol ratio of 1.67 [13]. |

Table 1. Cont.

| Active Metals | Supports | Promoters | Sample | Comments |
|--------------------|---|-----------|--------|---|
| | Al ₂ O ₃ | La | | Ni metal can be better dispersed by La [48]. |
| | Al ₂ O ₃ | Ag | | The best glycerol conversion (40.7%) and high yield of H ₂ (32%) were observed for Ag-Ni/Al ₂ O ₃ . This result can be ascribed to the smaller crystallite size of Ag in Ag-Ni/Al ₂ O ₃ , which was beneficial for metal dispersion [57]. |
| | Al ₂ O ₃ | Re | | Approximately 61% and 56% of glycerol conversion and hydrogen yield were observed for 5% Re-Ni/CaO, respectively. For 15% Ni/CaO, the conversion of glycerol and H ₂ yield are lower, being 35 and 30%, respectively. The addition of Re increases the acidic sites of the catalyst and promoted the adsorption of OH group of the glycerol onto the surface of catalyst [54]. |
| Rh, Ni and Co | ZrO ₂ -TiO ₂ | | | Rh showed the highest activity, while the activity of Co was the lowest [4]. |
| Rh, Ru, Ir, Pd, Pt | MgO-Al ₂ O ₃ | | | The catalytic activity followed the order: Rh > Ru > Ir > Pd > Pt [49]. |
| Rh | CeO ₂ , and ZrO ₂ | | | Rh/ZrO ₂ deactivated faster than Rh/CeO ₂ , due to the sintering of Rh metals and coke formation [15]. |

4. Conclusions and Future Perspectives

This review summarized the recent advance of dry reforming of ethanol and glycerol in the presence of various catalysts. Temperatures showed a positive effect on conversion, while CO₂/(ethanol or glycerol) ratio showed a different trend. The highest glycerol conversion can be maintained at CO₂/glycerol ratios of 1–2, while, for the case of ethanol reforming, the CO₂/ethanol ratios around 1.4 seem to be the optimum. The H₂/CO ratio also decreased with CO₂/glycerol ratio increasing due to the reverse WGS taking place simultaneously. For dry reforming of both compounds, the intermediate CH₄ was regarded as the main primary intermediate from the direct decomposition of ethanol and glycerol, which can be then reformed into H₂ and CO. The active metals, promoters, and supports were summarized in Figure 13. Ni based catalysts have shown their possible application in dry reforming of ethanol and glycerol, while deactivation issues due to the formation of carbon on the surface of catalyst and sintering of active metals hindered its wide application. Various promoters such as La and Ce have been proven to enhance Ni performance. Briefly, the boosted performance of the promoted catalysts is ascribed to: (i) Strong metal-support interaction: encapsulation of active metal nanoparticles by supports, (ii) Mobile oxygen species and creation of oxygen vacancies introduced by promoters mitigating coke formation.

IUPAC Periodic Table of Elements

| Key: | | | | | | | | | | | | | | | | | | | | | | | | | | | | | |
|---------------|----|--------|----|------------------------|-------------|-----|----|-----|----|-----|----|-----|----|-----|----|-----|-----|-----|----|----|----|-----|----|-----|----|-----|----|-----|----|
| atomic number | | Symbol | | standard atomic weight | | | | | | | | | | | | | | | | | | | | | | | | | |
| 1 | H | | | | | | | | | | | | | | | | 2 | | | | | | | | | | | | |
| 3 | Li | 4 | Be | | | | | | | | | | | | | | 10 | | | | | | | | | | | | |
| 11 | Na | 12 | Mg | | | | | | | | | | | | | | 18 | | | | | | | | | | | | |
| 19 | K | 20 | Ca | 21 | Sc | 22 | Ti | 23 | V | 24 | Cr | 25 | Mn | 26 | Fe | 27 | 28 | 29 | 30 | 31 | 32 | 33 | 34 | 35 | 36 | | | | |
| 37 | Rb | 38 | Sr | 39 | Y | 40 | Zr | 41 | Nb | 42 | Mo | 43 | Tc | 44 | Ru | 45 | 46 | 47 | 48 | 49 | 50 | 51 | 52 | 53 | 54 | | | | |
| 55 | Cs | 56 | Ba | 57–71 | Lanthanoids | 72 | Hf | 73 | Ta | 74 | W | 75 | Re | 76 | Os | 77 | 78 | 79 | 80 | 81 | 82 | 83 | 84 | 85 | 86 | | | | |
| 87 | Fr | 88 | Ra | 89–103 | actinoids | 104 | Rf | 105 | Db | 106 | Sg | 107 | Bh | 108 | Hs | 109 | 110 | 111 | | | | | | | | | | | |
| 57 | La | 58 | Ce | 59 | Pr | 60 | Nd | 61 | Pm | 62 | Sm | 63 | Eu | 64 | Gd | 65 | Tb | 66 | Dy | 67 | Ho | 68 | Er | 69 | Tm | 70 | Yb | 71 | Lu |
| 89 | Ac | 90 | Th | 91 | Pa | 92 | U | 93 | Np | 94 | Pu | 95 | Am | 96 | Cm | 97 | Bk | 98 | Cf | 99 | Es | 100 | Fm | 101 | Md | 102 | No | 103 | Lr |

Figure 13. The elements for the catalysts used in dry reforming. Red: Active components; Pink: Support; Yellow: Promoters.

The future foresees a great deal of possibilities for CO₂ reforming reactions as a direct route to tackle CO₂ emissions. Perhaps the industrial application of dry reforming remains as the biggest challenge for this technology nowadays. In fact, very few attempts of commercializing dry reforming plants have been conducted so far with the CALCOR process (a reforming process combined with CO₂ recovery and CO purification) patented by caloric being one of the first successful stories [58]. The development of advanced catalysts with high activity, selectivity, and, more importantly, stability constitute the principal bottleneck for the implementation of dry reforming reaction unit in realistic applications. Herein, the directions seem to go through the combination of engineered catalysts with the addition of promoters, multiple active phases, and sacrificial agents to avoid deactivation with cleverly designed regeneration strategies. At lab-scale, we have identified the need to conduct rigorous studies using realistic reforming mixtures (i.e., containing sulphur impurities)—this an effort that the

academic community should embrace to ensure a solid design of scalable high-performing catalysts. In any case, there is a lot of room for research in this promising area of catalysis for CO₂ valorization, and this mini-review just intends to be an introductory quick-guide to selected dry reforming reactions showcasing their potential contribution in the next generation of zero-carbon catalytic processes.

Author Contributions: Conceptualization, J.Y.; writing—original draft preparation, J.Y., T.R.R.; writing—review and editing, J.A.O.

Funding: This research was funded by the National Natural Science Foundation of China (NSFC)(51806078), and the Foundation of State Key Laboratory of Coal Combustion(FSKLCCB1904), the Royal society with the Grants EP/R512904/1 and RSGR1180353. The APC was funded by 51806078.

Conflicts of Interest: The authors declare no conflict of interest.

References

1. Joos, F.; Spahni, R. Rates of change in natural and anthropogenic radiative forcing over the past 20,000 years. *Proc. Natl. Acad. Sci. USA* **2008**, *105*, 1425–1430. [CrossRef] [PubMed]
2. Le Quéré, C.; Andrew, R.M.; Canadell, J.G.; Sitch, S.; Korsbakken, J.L.; Peters, G.P.; Manning, A.C.; Boden, T.A.; Tans, P.P.; Houghton, R.A.; et al. Global Carbon Budget 2016. *Earth Syst. Sci. Data* **2016**, *8*, 605–649. [CrossRef]
3. Garside, M. Ethanol Fuel Production in Top Countries 2018. Available online: <https://www.statista.com/statistics/281606/ethanol-production-in-selected-countries/> (accessed on 29 October 2019).
4. Bac, S.; Say, Z.; Kocak, Y.; Ercan, K.E.; Harfouche, M.; Ozensoy, E.; Avci, A.K. Exceptionally active and stable catalysts for CO₂ reforming of glycerol to syngas. *Appl. Catal. B Environ.* **2019**, *256*, 117808. [CrossRef]
5. Li, Z.; Yan, J.; Sun, J.; Xu, P.; Ma, C.; Gao, C. Production of value-added chemicals from glycerol using in vitro enzymatic cascades. *Commun. Chem.* **2018**, *1*, 71. [CrossRef]
6. Pardo-Planas, O.; Atiyeh, H.K.; Phillips, J.R.; Aichele, C.P.; Mohammad, S. Process simulation of ethanol production from biomass gasification and syngas fermentation. *Bioresour. Technol.* **2017**, *245*, 925–932. [CrossRef]
7. Roy, P.; Dias, G. Prospects for pyrolysis technologies in the bioenergy sector: A review. *Renew. Sustain. Energy Rev.* **2017**, *77*, 59–69. [CrossRef]
8. Li, S.; Savage, P.E.; Guo, L. Stability and activity maintenance of sol-gel Ni-MxOy (M = Ti, Zr, Ta) catalysts during continuous gasification of glycerol in supercritical water. *J. Supercrit. Fluids* **2019**, *148*, 137–147. [CrossRef]
9. Hashemi, H.; Christensen, J.M.; Glarborg, P. High-pressure pyrolysis and oxidation of ethanol. *Fuel* **2018**, *218*, 247–257. [CrossRef]
10. Bellido, J.D.A.; Tanabe, E.Y.; Assaf, E.M. Carbon dioxide reforming of ethanol over Ni/Y₂O₃–ZrO₂ catalysts. *Appl. Catal. B Environ.* **2009**, *90*, 485–488. [CrossRef]
11. Bahari, M.B.; Phuc, N.H.H.; Alenazey, F.; Vu, K.B.; Ainirazali, N.; Vo, D.-V.N. Catalytic performance of La-Ni/Al₂O₃ catalyst for CO₂ reforming of ethanol. *Catal. Today* **2017**, *291*, 67–75. [CrossRef]
12. Tavanarad, M.; Meshkani, F.; Rezaei, M. Production of syngas via glycerol dry reforming on Ni catalysts supported on mesoporous nanocrystalline Al₂O₃. *J. CO₂ Util.* **2018**, *24*, 298–305. [CrossRef]
13. Siew, K.W.; Lee, H.C.; Gimbin, J.; Chin, S.Y.; Khan, M.R.; Taufiq-Yap, Y.H.; Cheng, C.K. Syngas production from glycerol-dry(CO₂) reforming over La-promoted Ni/Al₂O₃ catalyst. *Renew. Energy* **2015**, *74*, 441–447. [CrossRef]
14. Da Silva, A.M.; de Souza, K.R.; Jacobs, G.; Graham, U.M.; Davis, B.H.; Mattos, L.V.; Noronha, F.B. Steam and CO₂ reforming of ethanol over Rh/CeO₂ catalyst. *Appl. Catal. B Environ.* **2011**, *102*, 94–109. [CrossRef]
15. Su, B.P.; Zafer, S.; Selin, B.; Emrah, O.; Ahmet, K. Dry reforming of glycerol over Rh-based ceria and zirconia catalysts: New insights on catalyst activity and stability. *Appl. Catal. A Gen.* **2018**, *564*, 157–171.
16. Cimenti, M.; Hill, J. Thermodynamic analysis of solid oxide fuel cells operated with methanol and ethanol under direct utilization, steam reforming, dry reforming or partial oxidation conditions. *J. Power Sources* **2009**, *186*, 377–384. [CrossRef]
17. López Ortiz, A.; Pallares Sámano, R.B.; Meléndez Zaragoza, M.J.; Collins-Martínez, V. Thermodynamic analysis and process simulation for the H₂ production by dry reforming of ethanol with CaCO₃. *Int. J. Hydrog. Energy* **2015**, *40*, 17172–17179. [CrossRef]

18. Kale, G.R.; Kulkarni, B.D. Thermoneutral point analysis of ethanol dry autothermal reforming. *Chem. Eng. J.* **2010**, *165*, 864–873. [[CrossRef](#)]
19. Bahari, M.B.; Phuc, N.H.H.; Abdullah, B.; Alenazey, F.; Vo, D.-V.N. Ethanol dry reforming for syngas production over Ce-promoted Ni/Al₂O₃ catalyst. *J. Environ. Chem. Eng.* **2016**, *4*, 4830–4838. [[CrossRef](#)]
20. Bahari, M.B.; Goo, B.C.; Pham, T.L.M.; Siang, T.J.; Danh, H.T.; Ainirazali, N.; Vo, D.-V.N. Hydrogen-rich Syngas Production from Ethanol Dry Reforming on La-doped Ni/Al₂O₃ Catalysts: Effect of Promoter Loading. *Procedia Eng.* **2016**, *148*, 654–661. [[CrossRef](#)]
21. Wang, W.; Wang, Y. Dry reforming of ethanol for hydrogen production: Thermodynamic investigation. *Int. J. Hydrog. Energy* **2009**, *34*, 5382–5389. [[CrossRef](#)]
22. Bej, B.; Pradhan, N.C.; Neogi, S. Production of hydrogen by steam reforming of ethanol over alumina supported nano-NiO/SiO₂ catalyst. *Catal. Today* **2014**, *237*, 80–88. [[CrossRef](#)]
23. Le Saché, E.; Santos, J.L.; Smith, T.J.; Centeno, M.A.; Arellano-Garcia, H.; Odriozola, J.A.; Reina, T.R. Multicomponent Ni-CeO₂ nanocatalysts for syngas production from CO₂/CH₄ mixtures. *J. CO₂ Util.* **2018**, *25*, 68–78. [[CrossRef](#)]
24. Le Saché, E.; Pastor-Pérez, L.; Watson, D.; Sepúlveda-Escribano, A.; Reina, T.R. Ni stabilised on inorganic complex structures: Superior catalysts for chemical CO₂ recycling via dry reforming of methane. *Appl. Catal. B Environ.* **2018**, *236*, 458–465. [[CrossRef](#)]
25. Stroud, T.; Smith, T.J.; Le Saché, E.; Santos, J.L.; Centeno, M.A.; Arellano-Garcia, H.; Odriozola, J.A.; Reina, T.R. Chemical CO₂ recycling via dry and bi reforming of methane using Ni-Sn/Al₂O₃ and Ni-Sn/CeO₂-Al₂O₃ catalysts. *Appl. Catal. B Environ.* **2018**, *224*, 125–135. [[CrossRef](#)]
26. Bej, B.; Bepari, S.; Pradhan, N.C.; Neogi, S. Production of hydrogen by dry reforming of ethanol over alumina supported nano-NiO/SiO₂ catalyst. *Catal. Today* **2017**, *291*, 58–66. [[CrossRef](#)]
27. Wei, Y.; Cai, W.; Deng, S.; Li, Z.; Yu, H.; Zhang, S.; Yu, Z.; Cui, L.; Qu, F. Efficient syngas production via dry reforming of renewable ethanol over Ni/KIT-6 nanocatalysts. *Renew. Energy* **2020**, *145*, 1507–1516. [[CrossRef](#)]
28. Zawadzki, A.; Bellido, J.D.A.; Lucrédio, A.F.; Assaf, E.M. Dry reforming of ethanol over supported Ni catalysts prepared by impregnation with methanolic solution. *Fuel Process. Technol.* **2014**, *128*, 432–440. [[CrossRef](#)]
29. Fedotov, A.S.; Antonov, D.O.; Bukhtenko, O.V.; Uvarov, V.I.; Kriventsov, V.V.; Tsodikov, M.V. The role of aluminum in the formation of Ni–Al–Co-containing porous ceramic converters with high activity in dry and steam reforming of methane and ethanol. *Int. J. Hydrog. Energy* **2017**, *42*, 24131–24141. [[CrossRef](#)]
30. Fayaz, F.; Nga, N.T.A.; Pham, T.L.M.; Danh, H.T.; Abdullah, B.; Setiabudi, H.D.; Vo, D.-V.N. Hydrogen production from ethanol dry reforming over lanthania-promoted Co/Al₂O₃ catalyst. *IIUM Eng. J.* **2018**, *19*, 24–33. [[CrossRef](#)]
31. Fayaz, F.; Danh, H.T.; Nguyen-Huy, C.; Vu, K.B.; Abdullah, B.; Vo, D.-V.N. Promotional Effect of Ce-dopant on Al₂O₃-supported Co Catalysts for Syngas Production via CO₂ Reforming of Ethanol. *Procedia Eng.* **2016**, *148*, 646–653. [[CrossRef](#)]
32. Fayaz, F.; Bahari, M.B.; Pham, T.L.; Nguyen-Huy, C.; Setiabudi, H.D.; Abdullah, B.; Vo, D.-V.N. Hydrogen-Rich Syngas Production via Ethanol Dry Reforming over Rare-Earth Metal-Promoted Co-based Catalysts. In *Recent Advancements in Biofuels and Bioenergy Utilization*; Springer: Berlin/Heidelberg, Germany, 2018; pp. 177–204.
33. Cao, D.; Zeng, F.; Zhao, Z.; Cai, W.; Li, Y.; Yu, H.; Zhang, S.; Qu, F. Cu based catalysts for syngas production from ethanol dry reforming: Effect of oxide supports. *Fuel* **2018**, *219*, 406–416. [[CrossRef](#)]
34. Cao, D.; Cai, W.; Li, Y.; Li, C.; Yu, H.; Zhang, S.; Qu, F. Syngas Production from Ethanol Dry Reforming over Cu/Ce_{0.8}Zr_{0.2}O₂ Catalyst. *Catal. Lett.* **2017**, *147*, 2929–2939. [[CrossRef](#)]
35. Shafiqah, M.-N.N.; Nguyen, T.D.; Jun, L.N.; Bahari, M.B.; Phuong, P.T.; Abdullah, B.; Vo, D.-V.N. Production of syngas from ethanol CO₂ reforming on La-doped Cu/Al₂O₃: Impact of promoter loading. In *AIP Conference Proceedings*; AIP Publishing: College Park, MD, USA, 2019; Volume 2124, p. 020011.
36. Chen, Q.; Cai, W.; Liu, Y.; Zhang, S.; Li, Y.; Huang, D.; Wang, T.; Li, Y. Synthesis of Cu-Ce_{0.8}Zr_{0.2}O₂ catalyst by ball milling for CO₂ reforming of ethanol. *J. Saudi Chem. Soc.* **2019**, *23*, 111–117. [[CrossRef](#)]
37. Aupretre, F.; Descorme, C.; Duprez, D.; Casanave, D.; Uzio, D. Ethanol steam reforming over Mg_xNi_{1-x}Al₂O₃ spinel oxide-supported Rh catalysts. *J. Catal.* **2005**, *233*, 464–477. [[CrossRef](#)]
38. Mavrikakis, M.; Barteau, M.A. Oxygenate reaction pathways on transition metal surfaces. *J. Mol. Catal. A Chem.* **1998**, *131*, 135–147. [[CrossRef](#)]

39. Zhao, S.; Cai, W.; Li, Y.; Yu, H.; Zhang, S.; Cui, L. Syngas production from ethanol dry reforming over Rh/CeO₂ catalyst. *J. Saudi Chem. Soc.* **2018**, *22*, 58–65. [[CrossRef](#)]
40. Wu, X.; Kawi, S. Rh/Ce-SBA-15: Active and stable catalyst for CO₂ reforming of ethanol to hydrogen. *Catal. Today* **2009**, *148*, 251–259. [[CrossRef](#)]
41. Drif, A.; Bion, N.; Brahmi, R.; Ojala, S.; Pirault-Roy, L.; Turpeinen, E.; Seelam, P.K.; Keiski, R.L.; Epron, F. Study of the dry reforming of methane and ethanol using Rh catalysts supported on doped alumina. *Appl. Catal. A Gen.* **2015**, *504*, 576–584. [[CrossRef](#)]
42. Blanchard, J.; Oudghiri-Hassani, H.; Abatzoglou, N.; Jankhah, S.; Gitzhofer, F. Synthesis of nanocarbons via ethanol dry reforming over a carbon steel catalyst. *Chem. Eng. J.* **2008**, *143*, 186–194. [[CrossRef](#)]
43. Jankhah, S.; Abatzoglou, N.; Gitzhofer, F. Thermal and catalytic dry reforming and cracking of ethanol for hydrogen and carbon nanofilaments' production. *Int. J. Hydrog. Energy* **2008**, *33*, 4769–4779. [[CrossRef](#)]
44. De Oliveira-Vigier, K.; Abatzoglou, N.; Gitzhofer, F. Dry-Reforming of Ethanol in the Presence of a 316 Stainless Steel Catalyst. *Can. J. Chem. Eng.* **2005**, *83*, 978–984. [[CrossRef](#)]
45. Kale, G.R.; Kulkarni, B.D. Thermodynamic analysis of dry autothermal reforming of glycerol. *Fuel Process. Technol.* **2010**, *91*, 520–530. [[CrossRef](#)]
46. Wang, S.; Wang, Q.; Song, X.; Chen, J. Dry autothermal reforming of glycerol with in situ hydrogen separation via thermodynamic evaluation. *Int. J. Hydrog. Energy* **2017**, *42*, 838–847. [[CrossRef](#)]
47. Wang, X.; Li, M.; Wang, M.; Wang, H.; Li, S.; Wang, S.; Ma, X. Thermodynamic analysis of glycerol dry reforming for hydrogen and synthesis gas production. *Fuel* **2009**, *88*, 2148–2153. [[CrossRef](#)]
48. Siew, K.W.; Lee, H.C.; Gim bun, J.; Cheng, C.K. Production of CO-rich hydrogen gas from glycerol dry reforming over La-promoted Ni/Al₂O₃ catalyst. *Int. J. Hydrog. Energy* **2014**, *39*, 6927–6936. [[CrossRef](#)]
49. Tavanarad, M.; Meshkani, F.; Rezaei, M. Synthesis and Application of Noble Metal Nanocatalysts Supported on MgAl₂O₄ in Glycerol Dry Reforming Reaction. *Catal. Lett.* **2018**, *148*, 164–172. [[CrossRef](#)]
50. Hua, C.L.; Siew, K.W.; Gim bun, J.; Cheng, C.K. Synthesis and characterisation of cement clinker-supported nickel catalyst for glycerol dry reforming. *Chem. Eng. J.* **2014**, *255*, 245–256.
51. Lee, H.C.; Siew, K.W.; Khan, M.R.; Chin, S.Y.; Gim bun, J.; Cheng, C.K. Catalytic performance of cement clinker supported nickel catalyst in glycerol dry reforming. *J. Energy Chem.* **2014**, *23*, 645–656. [[CrossRef](#)]
52. Siew, K.W.; Lee, H.C.; Gim bun, J.; Cheng, C.K. Characterization of La-promoted Ni/Al₂O₃ catalysts for hydrogen production from glycerol dry reforming. *J. Energy Chem.* **2014**, *23*, 15–21. [[CrossRef](#)]
53. Siew, K.W.; Lee, H.C.; Khan, M.R.; Gim bun, J.; Cheng, C.K. CO₂ reforming of glycerol over La-Ni/Al₂O₃ catalyst: A longevity evaluative study. *J. Energy Chem.* **2015**, *24*, 366–373. [[CrossRef](#)]
54. Mohd Arif, N.N.; Abidin, S.Z.; Osazuwa, O.U.; Vo, D.-V.N.; Azizan, M.T.; Taufiq-Yap, Y.H. Hydrogen production via CO₂ dry reforming of glycerol over ReNi/CaO catalysts. *Int. J. Hydrog. Energy* **2019**, *44*, 20857–20871. [[CrossRef](#)]
55. Harun, N.; Abidin, S.Z.; Osazuwa, O.U.; Yun, T.Y.; Azizan, M.T. Hydrogen production from glycerol dry reforming over Ag-promoted Ni/Al₂O₃. *Int. J. Hydrog. Energy* **2019**, *44*, 213–225. [[CrossRef](#)]
56. Qu, F.; Wei, Y.; Cai, W.; Yu, H.; Li, Y.; Zhang, S.; Li, C. Syngas production from carbon dioxide reforming of ethanol over Ir/Ce_{0.75}Zr_{0.25}O₂ catalyst: Effect of calcination temperatures. *Energy Fuels* **2018**, *32*, 2104–2116. [[CrossRef](#)]
57. Harun, N.; Gim bun, J.; Azizan, M.T.; Abidin, S.Z. Characterization of Ag-promoted Ni/SiO₂ catalysts for syngas production via carbon dioxide (CO₂) dry reforming of glycerol. *Bull. Chem. React. Eng. Catal.* **2016**, *11*, 220–229. [[CrossRef](#)]
58. German, K.; Von, L.J. Process for Obtaining Carbon Monoxide. German Patent No. DE3617280A1, 23 May 1986.

